Catal Lett (2012) 142:718–727
DOI 10.1007/s10562-012-0830-4

NiW and NiRu Bimetallic Catalysts for Ethylene Steam Reforming: Alternative Mechanisms for Sulfur Resistance

Meghana Rangan · Matthew M. Yung · J. Will Medlin

Received: 31 January 2012 / Accepted: 13 April 2012 / Published online: 4 May 2012

Abstract Previous investigations of Ni-based catalysts for the steam reforming of hydrocarbons have indicated that the addition of a second metal can reduce the effects of sulfur poisoning. Two systems that have previously shown promise for such applications, NiW and NiRu, are considered here for the steam reforming of ethylene, a key component of biomass derived tars. Monometallic and bimetallic Al_2O_3-supported Ni and W catalysts were employed for ethylene steam reforming in the presence and absence of sulfur. The NiW catalysts were less active than Ni in the absence of sulfur, but were more active in the presence of 50 ppm H_2S. The mechanism for the W-induced improvements in sulfur resistance appears to be different from that for Ru in NiRu. To probe reasons for the sulfur resistance of NiRu, the adsorption of S and C_2H_4 on several bimetallic NiRu alloy surfaces ranging from 11 to 33 % Ru was studied using density functional theory (DFT). The DFT studies reveal that sulfur adsorption is generally favored on hollow sites containing Ru. Ethylene preferentially adsorbs atop the Ru atom in all the NiRu (111) alloys investigated. By comparing trends across the various bimetallic models considered, sulfur adsorption was observed to be correlated with the density of occupied states near the Fermi level while C_2H_4 adsorption was correlated with the number of unoccupied states in the d-band. The diverging mechanisms for S and C_2H_4 adsorption allow for bimetallic surfaces such as NiRu that enhance ethylene binding without accompanying increases in sulfur binding energy. In contrast, bimetallics such as NiSn and NiW appear to decrease the affinity of the surface for both the reagent and the poison.

Keywords Electronic structure · Sulfur · Ethylene · NiRu · DFT

1 Introduction

Supported Ni catalysts are well known for their high activity for the steam reforming of hydrocarbons. However, the lifetime of these catalysts is greatly reduced by sulfur poisoning. Although desulfurization of the reforming feed stream can potentially be used to avoid catalyst poisoning, such reactions are complex and not very cost effective [1]. Development of sulfur-resistant or sulfur-tolerant catalysts is an attractive alternative [2, 3]. It is widely accepted that modifying the electronic properties of a metal catalyst by adding a second metal to form a bimetallic is one of the best ways to modify its catalytic properties [4–8]. For instance, a Ni-W/Al_2O_3 catalyst maintains its activity for a longer period of time in the presence of sulfur than a monometallic Ni/Al_2O_3 catalyst during the steam reforming of gasoline [9]. Strohm et al. [10] have found that the addition of Ni to a Rh/CeO_2–Al_2O_3 catalyst greatly improves its resistance to sulfur poisoning during the reforming of jet fuel. Likewise, it has been reported that a Ni–Re/Al_2O_3 catalyst maintains activity longer than a pure Ni catalyst during the steam reforming of sulfur-containing fuels [11, 12]. The addition of a second metal (such as Sn

Electronic supplementary material The online version of this article (doi:10.1007/s10562-012-0830-4) contains supplementary material, which is available to authorized users.

M. Rangan · J. W. Medlin (✉)
Department of Chemical and Biological Engineering, University of Colorado, Boulder, CO 80309, USA
e-mail: will.medlin@colorado.edu

M. M. Yung
National Bioenergy Center, National Renewable Energy Laboratory, Golden, CO 80401, USA

or Au) to a Ni catalyst not only affects S adsorption but can also significantly change the energetics of coking reactions [13, 14]. Studies have shown that a Ru-doped Ni/Al_2O_3 catalyst is much more resistant to deactivation due to carbon deposition than a pure Ni catalyst [15, 16].

In previous work, we used ethylene as a probe molecule to experimentally study the activities of various Ni bimetallic catalysts [17]. We found that C_2H_4 conversion in both the presence and absence of sulfur is much higher on the NiRu bimetallic catalyst compared to a monometallic Ni catalyst. The NiRu bimetallic catalyst was also more active for the reforming of ethylene, methane, and benzene in a model synthesis gas stream both in the presence and absence of sulfur. We furthermore reported on preliminary density functional theory (DFT) calculations which indicated that NiRu bimetallics were characterized by stronger binding of ethylene and sulfur, but with promotion of ethylene binding (and subsequent decomposition) being much stronger [17].

In this paper, we explore the mechanism for sulfur resistance during ethylene reforming on NiRu bimetallic catalysts. Furthermore, we compare the mechanism for sulfur resistance to that on another bimetallic catalyst that has previously been employed for improving sulfur resistance during hydrocarbon reforming, NiW. In particular, we investigate structure–property relations for NiRu bimetallic surfaces to probe the mechanism by which addition of Ru alters the interaction of ethylene and sulfur with the surface. Across a range of bimetallic surface models, we explore how ethylene and sulfur adsorption energies are affected by the change in the electronic structure of a Ni catalyst caused by the addition of Ru [4]. Rather than attempting to determine the precise NiRu surface structures present during reaction, the focus is on identifying explanations for the enhancement of adsorption energy for ethylene without a corresponding increase in the adsorption energy of sulfur. Understanding the adsorption of simple adsorbates like S and C_2H_4 on NiRu surfaces is a key step towards understanding the surface kinetics and detailed mechanisms involved in steam reforming of hydrocarbons in the presence of sulfur on bimetallic Ni surfaces.

2 Methods

2.1 DFT Calculations

Total energies of adsorbed sulfur and ethylene on various NiRu surfaces were obtained from DFT calculations performed using the Vienna ab initio simulation package [18, 19]. The Kohn–Sham one-electron valence states were expanded in a plane wave basis set using the projector augmented wave method [20]. A cutoff energy of 350 eV was used in the expansion of the plane wave basis set. The Perdew–Wang (PW91) generalized gradient approximation functional was employed to calculate the exchange–correlation energy [21]. A periodic supercell was used to model the bimetallic NiRu(111) surfaces. In order to determine the equilibrium lattice constant, the bulk bimetallic NiRu was geometrically optimized with a $11 \times 11 \times 11$ Monkhorst–Pack k-point mesh to obtain the lowest energy lattice constant [22]. In all the calculations performed, the top two layers of the slab were relaxed and the Brillouin zone was sampled using a $7 \times 7 \times 1$ Monkhorst–Pack k point mesh [22].

Previous studies have indicated that Ni and Ru atoms in a NiRu alloy interact with each other to form a fairly homogeneous alloy [23]. Thus, the bimetallic NiRu(111) slabs we examined contained varying proportions of Ni and Ru atoms both on the surface and in the bulk. Alloy naming corresponds to the concentration of Ru and Ni in the NiRu alloy (e.g. $Ru_{0.25}Ni_{0.75}$ slab contains 25 % Ru and 75 % Ni). We studied S and C_2H_4 coverage effects by examining the following adsorbate (C_2H_4 and S) coverages −1/16ML, 1/8ML, 1/4ML and 1/2ML—on a $Ru_{0.25}Ni_{0.75}(111)$ surface. The $Ru_{0.25}Ni_{0.75}$ alloy consists of 2×2 unit cells with a Ni to Ru ratio of 3:1 in each of its 4 layers. The effect of Ru coverage was investigated by calculating S and C_2H_4 adsorption on three different NiRu alloys with varying concentrations of Ru–$Ru_{0.33}Ni_{0.67}(111)$ (%Ru = 33), $Ru_{0.22}Ni_{0.78}(111)$ (%Ru = 22) and $Ru_{0.11}Ni_{0.89}(111)$ (%Ru = 11) (see supporting information for details). We used an adsorbate coverage of 1/9ML on each of the 3 alloys. We also studied adsorption trends for the same sulfur and ethylene coverages—1/16ML, 1/8ML, 1/4ML and 1/2ML—on $Ru_{0.25}Ni_{0.75}(100)$. The S and C_2H_4 adsorption energies in all cases were calculated by subtracting the adsorbate/substrate energy from the reference energy. A positive reaction energy indicates an exothermic reaction while a negative reaction energy implies an endothermic reaction.

Details of the electronic structure of the NiRu alloys were obtained by projecting the density of states (DOS) onto individual atoms. The d-band centers reported in this paper are the weighted average of the d-band and are referenced to the Fermi level [24]. The DOS plots shown in this paper are also referenced to the Fermi level.

2.2 Experimental Methods

A series of catalysts were prepared via incipient-wetness impregnation. During the synthesis, the precursors were dissolved into an aqueous solution that was then added, dropwise, to the catalyst support to fill the appropriate pore volume. Catalyst precursors for nickel and tungsten were

nickel nitrate hexahydrate, $Ni(NO_3)_2{\cdot}6H_2O$ (Aldrich), and ammonium metatungstate, $(NH_4)_6W_{12}O_{39}$ (Aldrich), respectively. The catalyst supports that were used were fluidizable and attrition-resistant so that the materials could be used in a fluidizing environment as necessary. The support was alpha-alumina (α-Al_2O_3, Saint Gobain Norpro), a proprietary support from *CoorsTek Ceramics* which consists of 90 % α-Al_2O_3 and a specified mixture of other oxides. In instances when more than one impregnation was used, the impregnated support was dried in air at 110 °C for at least 3 h, to evaporate water and restore pore volume, before additional impregnations were performed. Following impregnations, the catalysts were calcined by heating in air at a rate of 10 K/min to 900 °C and held for 3 h. Catalyst naming corresponds to the molar ratio between Ni and the promoter (e.g. $W_{0.33}Ni/\alpha$-Al_2O_3 corresponds to 6 %Ni/α-Al_2O_3 with a 0.33:1 W:Ni molar ratio).

H_2 chemisorption was conducted at 40 °C on a Quantachrome Autosorb instrument. Catalyst dispersion was calculated assuming one adsorbed H atom per surface Ni atom, with a Ni surface area of 1.2×10^{19} atoms/m^2 based on an equal distribution of the three lowest index planes of nickel (fcc) [25, 26]. Temperature-programmed reduction (TPR) was done on 200 mg of sample using 10 %H_2/Ar and ramping from 50 to 850 °C at 10 °C/min and H_2 consumption was measured using a TCD to reference the reactor inlet stream to the gas at the reactor exit, after being sent through molecular sieves to remove moisture. X-ray diffraction (XRD) scans from 20 to 80° 2θ were performed on a Scintag diffractometer using a step size of 0.02°. Electron microscopy was conducted using a field emission scanning electron microscope (JSM-7401F). X-ray absorption fine structure (XAFS) spectroscopy was performed at DuPont-Northwestern-Dow (DND) collaborative Access Team (CAT) beamline 5-BM-D (BM = bending magnet, http://www.dnd.aps.anl.gov/) at the Advanced Photon Source, Argonne National Laboratory. The XAFS spectra was analyzed using the Athena software package as described previously by Yung et al. [27–30].

Reactions on powdered catalyst samples were conducted in a fixed-bed reactor, with the catalyst held in place between quartz wool plugs within a quartz, U-tube reactor and heated by an electric furnace. Gas flow rates were controlled by mass flow controllers (MKS Instruments) and steam was introduced by adjusting helium flow through a gas washing bottle filled with DI water and heated in an oil bath to 70 °C. All lines downstream of the bubbler were heat traced (>100 °C) to prevent condensation. The composition of the hot gas stream was measured using a Dycor Proline mass spectrometer. The reactor system had a bypass flow line for feed analysis before and after each reaction. Catalysts (175 mg) were heated from 25 to 900 °C at 10 °C/min in 10 % H_2/N_2, and then held at 900 °C for 30 min to pretreat the samples prior to reaction. All flow rates (dry) were 100 sccm in the reaction studies. Catalyst tests lasted 3 h, consisting of (i) 60 min exposure to reaction gases without H_2S, (ii) 30 min exposure to reaction gases with H_2S, and (iii) 90 min exposure to reaction gases without H_2S. Catalysts were examined for ethylene steam reforming (2 % C_2H_4, 50 ppm H_2S when included, 32 % H_2O and balance He). These reaction studies were performed at 900 °C.

3 Results and Discussion

3.1 Sulfur Resistant Ethylene Reforming on NiW Catalysts

3.1.1 Experimental Studies of Ethylene Steam Reforming

Bimetallic NiW catalysts have previously been found to improve the sulfur resistance during hydrocarbon reforming reactions. To our knowledge, they have not previously been investigated for ethylene reforming. Therefore, for the purposes of comparison to NiRu reforming catalysts, it is useful to briefly examine reactivity trends for a set of catalysts including supported Ni, W, and two different NiW bimetallic catalysts. Figure 1 shows ethylene conversion versus time on Ni/Al_2O_3, $W_{0.1}Ni/Al_2O_3$, $W_{0.33}Ni/Al_2O_3$ and W/Al_2O_3. Before H_2S was introduced, the trend in ethylene reforming activity was $Ni/Al_2O_3 > W_{0.1}Ni/Al_2O_3 > W_{0.33}Ni/Al_2O_3 > W/Al_2O_3$. The introduction of H_2S led to lower C_2H_4 conversion on all catalysts. The trend in ethylene conversion after the introduction of 50 ppm of H_2S was $W_{0.1}Ni/Al_2O_3 > W_{0.33}Ni/Al_2O_3 > Ni/Al_2O_3 > W/Al_2O_3$. The catalyst with lower tungsten loading, $W_{0.1}Ni/Al_2O_3$, showed higher activity than $W_{0.33}Ni/Al_2O_3$ both in the presence as well as the absence of H_2S in the feed stream, indicating that there is an optimum amount W required in the catalyst to improve its sulfur resistance, while very high loadings of W can significantly lower activity for C_2H_4 steam reforming. This is because W is inactive as a reforming catalyst as can be seen in Fig. 1. Upon the removal of H_2S, in the final hour of the reaction, the two NiW catalysts recovered activity at almost the same rate as the pure Ni catalyst. However, the two NiW catalysts showed higher conversions than the monometallic Ni catalyst even in this step of the reaction. The partial restoration of activity on all the catalysts following removal of H_2S suggests that H_2S caused a decrease in C_2H_4 conversion due both to reversible poisoning of the Ni sites and to irreversible changes in the catalyst structure or composition.

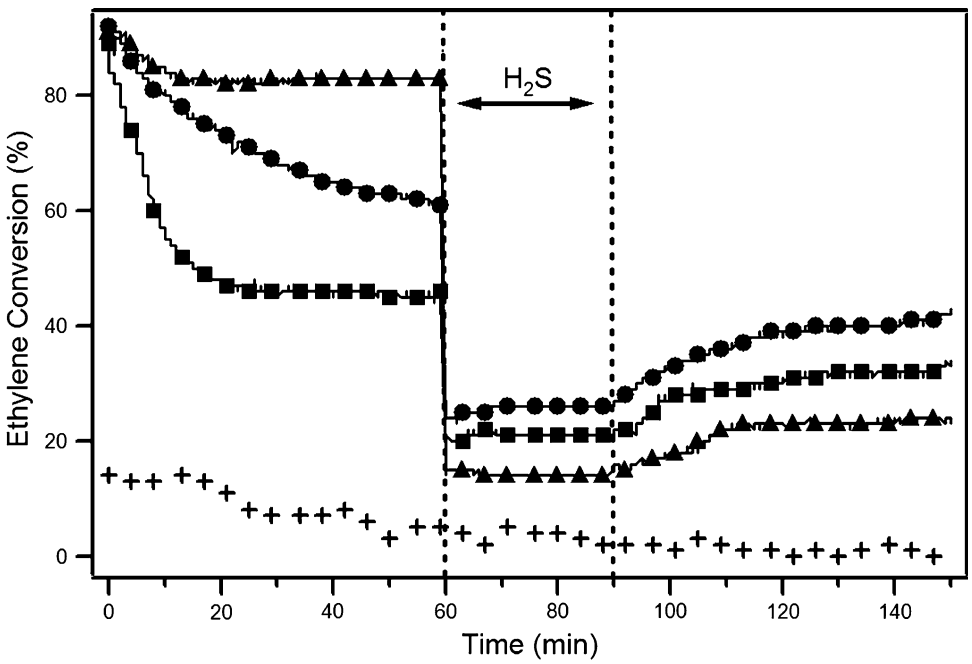

Fig. 1 Ethylene conversion versus time on Ni/Al_2O_3 (*filled triangle*), $W_{0.1}Ni/Al_2O_3$ (*filled circle*), $W_{0.33}Ni/Al_2O_3$ (*filled square*) and W/Al_2O_3 (+)

Catalysts were characterized in their as-synthesized, post-reduction, and post-reaction states using a variety of characterization techniques. Full details are provided in the supporting information, but an overview of key results is given here. Hydrogen chemisorption results showed that that the active catalyst surface area for the pure Ni catalyst was 55–60 % higher than that of the $W_{0.1}Ni$ catalyst in both the reduced and post-reaction state. The Ni dispersions of the $W_{0.1}Ni$ and $W_{0.33}Ni$ catalysts were more similar, with the $W_{0.1}Ni$ catalyst having approximately 15 % more active surface area. A drop in active surface area of more than 40 % was observed for all catalysts after reaction. SEM images (figure S3 of the supporting information) obtained for the Ni and $W_{0.1}Ni$ catalysts show particle growth during reaction that is consistent with the loss in dispersion.

Temperature programmed reduction results (figure S1 of the supporting information) for the various catalysts indicate that increasing W content was correlated with higher-temperature TPR peaks, indicating as expected that W decreases the reducibility of the catalyst. These findings are consistent with results from XRD (supporting figure S2), which indicate that the $W_{0.33}Ni$ catalysts retain a $NiWO_4$ peak and a WO_3 peak at 29.2 and 40.9°, respectively, in the reduced $W_{0.33}Ni/Al_2O_3$ catalyst. In the post-reaction samples, both the $W_{0.33}Ni$ and $W_{0.1}Ni$ catalysts exhibited more significant peaks attributed to $NiWO_4$ formation. Results from EXAFS (figure S4 of the supporting information) are generally consistent with the observations described above, with the $W_{0.33}Ni$ catalyst being associated with a Ni–O backscatter pair even in the reduced sample, with oxidation increasing in the post-reaction samples. Overall, the characterization results indicate that W lowers the availability of reducible, active sites in the Ni catalyst, and that though W improves sulfur resistance it comes at a cost of reduced sulfur-free activity.

3.1.2 Sulfur and Ethylene Adsorption on NiW Bimetallic Surfaces

We conducted preliminary DFT investigations of sulfur and ethylene adsorption on ordered NiW bimetallic surfaces for direct comparison to the studies indicated below. Both sulfur and ethylene adsorption are highly favorable in the W-containing sites of $W_{0.33}Ni_{0.67}(111)$ with adsorption energies favored by 1.07 and 0.55 eV, respectively, compared to Ni(111). On the other hand, the S adsorption energy is slightly less favorable on $W_{0.11}Ni_{0.89}(111)$ compared to Ni(111) by 0.12 and 0.07 eV, respectively. These results suggest that high W contents are associated with high sulfur and ethylene adsorption energies, in contrast with the experimental trends. As discussed in greater detail below, we hypothesize that this divergence is due to the fact that a homogeneous alloy is not a valid model for the experimental NiW catalysts. Differences in surface structure between different alloys makes development of a truly unified theory for the sulfur resistance of bimetallic catalysts difficult, as discussed in Sect. 3.3.

3.2 Sulfur Resistant Ethylene Reforming on NiRu Catalysts

3.2.1 *Experimental Studies of Ethylene Steam Reforming*

As discussed in the introduction, we have previously performed experimental investigations similar to those described in Sect. 3.1 using NiRu bimetallic catalysts for steam reforming of ethylene in the presence of H_2S [17]. Briefly, these investigations showed that NiRu catalysts (at loadings of both $Ru_{0.33}Ni$ and $Ru_{0.1}Ni$) showed higher activities for reforming of ethylene both in the absence and presence of 5 ppm H_2S. While H_2S lowered conversion on all catalysts, the rate was affected less on the NiRu bimetallics. Several techniques including TPR, XRD, SEM, and EXAFS were employed to demonstrate a significant interaction between bimetallic components. The NiRu catalysts were also observed to be more active both in the presence and absence of H_2S during reforming of a model biomass tar stream containing ethylene, methane, and benzene. In the sections below, we employ DFT calculations to compute trends in the adsorption of ethylene and sulfur on NiRu bimetallic surfaces with an aim of explaining reasons for the enhanced activity and sulfur resistance.

Note that in the experimental work reported here, NiW catalysts were exposed to a higher H_2S concentration (50 ppm) as compared to the NiRu catalysts in the previous study (5 ppm) [17]. While previous studies have generally shown that higher H_2S concentrations in this range result in decreased catalyst activity and more rapid deactivation [31], it is important to point out that NiW and NiRu bimetallic catalysts may have different ranges of effective sulfur resistance based on their different mechanisms for sulfur tolerance described below.

3.2.2 *Sulfur and Ethylene Adsorption on Ni and NiRu Bimetallic Surfaces*

A major focus of this paper is on studying how changes in the model for the NiRu bimetallic surface—including the surface structure, Ru content, and Ru distribution—affect the adsorption of ethylene on sulfur. It is useful to begin, however, by providing an overview of the general observations for adsorption of sulfur and ethylene on four surfaces: Ni(111), Ni(100), $Ru_{0.25}Ni_{0.75}$(111), and $Ru_{0.25}Ni_{0.75}$(100). Adsorption energies at three different surface coverages are shown in Tables 1 and 2. Considering these surfaces allows for comparing adsorption energy trends across surfaces and across compositions. For all surfaces, ethylene preferentially adsorbs in atop sites. From Table 1, it is apparent that ethylene binds significantly more strongly on the bimetallic surface than on pure Ni surfaces. The difference in binding energy depends to some extent on the surface structure and adsorbate coverage, but on average ethylene adsorption is found to be 0.3–0.4 eV more stable on the bimetallic surfaces.

Table 1 Adsorption energies (eV) of ethylene as a function of surface and coverage

Fractional coverage	Ni(111)	Ni_3Ru(111)	Ni(100)	Ni_3Ru(100)
1/16	−1.01	−1.10	−0.83	−1.24
1/8	−0.94	−1.10	−0.74	−1.23
1/4	−0.89	−1.37	−0.70	−1.21

Table 2 Adsorption energies (eV) of atomic sulfur as a function of surface and coverage

Fractional coverage	Ni(111)	Ni_3Ru(111)	Ni(100)	Ni_3Ru(100)
1/16	−6.10	−5.94	−6.82	−6.53
1/8	−6.07	−6.04	−6.80	−6.52
¼	−6.05	−6.17	−6.77	−6.66
½	−3.32	−3.84	−3.37	−3.07

Sulfur adsorbs in hollow sites on both the (111) and (100) surfaces of Ni and $Ru_{0.25}Ni_{0.75}$; in the case of the bimetallic surfaces, these sites include one Ru atom (Fig. 2). In contrast to the case of ethylene, sulfur adsorption is not noticeably favored on the bimetallic surfaces. In fact, for coverages of ¼ML and below, the average binding energy of sulfur is >0.10 eV more exothermic on the monometallic surface. Thus, whereas ethylene binding (and thus reactivity toward bond breaking reactions) is clearly favored on the bimetallic, sulfur binding is not stabilized. This is consistent with the finding that ethylene steam reforming activity on the bimetallic is improved both in the presence and absence of H_2S, but more so in the presence of H_2S.

It is useful to examine the sensitivity of the results presented above to varying contents and distributions of Ru in the bimetallic. Full details on these calculations are reported in the Supplementary Information. Table S3 compares the trends for S and C_2H_4 adsorption energies with varying Ru concentrations in the alloy. No clear trend was observed between S adsorption energy and Ru content, though S adsorption was found to be slightly weaker (by ~0.1 eV) for the surface that was the most dilute in Ru. In constrast, C_2H_4 adsorption became less exothermic (by ~0.2 eV) as we increased the Ru concentration in the slab from 11 % Ru to 33 % Ru. That is, the strongest ethylene adsorption is observed for the surface that is most dilute in Ru, such that isolated Ru atoms appear to be associated with strong ethylene adsorption. However, catalysts that

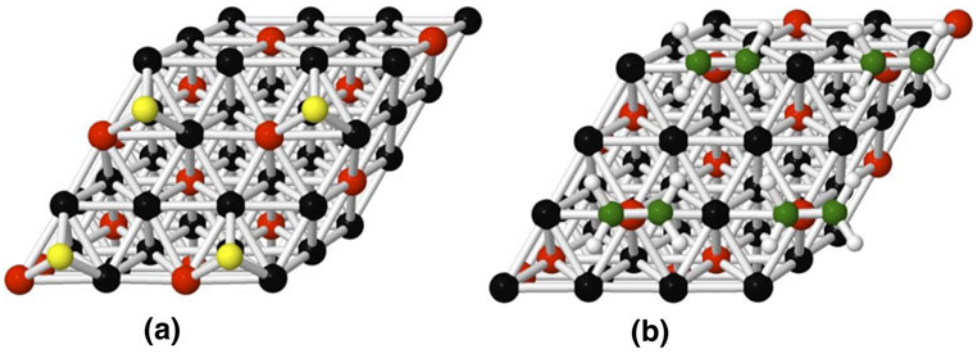

Fig. 2 **a** S adsorbed on the Ru hollow site of $Ru_{0.25}Ni_{0.75}(111)$ and **b** C_2H_4 adsorbed atop a Ru atom in $Ru_{0.25}Ni_{0.75}(111)$. The *black atoms* represent Ni, the *red atoms* represent Ru, the *green atoms* represent C, the *white atoms* represent H and the *yellow atoms* represent S

are highly dilute in Ru will have few of these active sites, a tradeoff remarked upon in a previous contribution [17].

The adsorption energies are also somewhat sensitive to the distribution of Ru within the bimetallic. The results for S and C_2H_4 adsorbed on homogeneous and simple inhomogeneous models (characterized by the presence of Ru–Ru bonds within the lattice) for $Ru_{0.25}Ni_{0.75}(111)$ are shown in Table S4 of the Supplementary Information. There is a general trend that the presence of Ru–Ru bonds weakens ethylene adsorption because ethylene prefers to bind to isolated surface Ru atoms. For S adsorption, there is no clear trend, with some inhomogeneous models strengthening binding and others weakening it. Despite the subtle variations with Ru content and distribution, there is one key overall conclusion: that regardless of the Ru composition and distribution conditions examined in these calculations, ethylene binding is significantly stabilized on the NiRu bimetallic surfaces, whereas sulfur adsorption generally is not. Nevertheless, the results of the calculations with different Ru loadings and distributions helps in developing a picture of the surface electronic characteristics that lead to desirable ethylene and sulfur adsorption energies, as discussed in the following section.

3.2.3 Electronic Effects on Binding

The results section above focuses on identifying binding energy trends for several NiRu bimetallic models. The focus of this section is to unify these results to identify the underlying explanations for observed trends for both sulfur and ethylene adsorption. The adsorption of sulfur compounds on transition metals has been widely studied and reviewed [32–35]. More specifically, sulfur adsorption on Ni surfaces and catalysts has been investigated both theoretically and experimentally [36–43]. The d-band center has been identified as often being a good indicator of the adsorbate–substrate bond strength and chemical reactivity [44]. However, on NiRu bimetallic surfaces, adsorption of S is complicated by the fact that two different types of metal atoms, Ru and Ni, can be present in the binding site. It is therefore expected that utilizing a single metric, such as the d-band center, may be problematic in correlation of binding energy trends. Supporting figure S7 shows the change in S adsorption energies with changing d-band center of the Ru atom in the NiRu alloys. We do not observe a linear decrease in S adsorption energy with increasing d-band center for this limited range of bimetallic surfaces. Similarly, there was no direct correlation between the S adsorption energy and the d-band center of the Ni atom (supporting Fig. S7). However, as suggested by Norskov et al., the adsorption of an atom or molecule on closely related transition metal surfaces cannot be explained in terms of the d-band center alone [45]. Studies by Hyman et al. [24] indicate that S adsorption on Pd(111) and Pd bimetallic surfaces is dependent on the width of the d-band and the DOS near the Fermi level. The DOS near the Fermi level is indicative of the number of occupied states available for bonding and the unoccupied states that reduce the anti-bonding repulsions.

As seen in Fig. 3, the width of the d-band of the Ni atom and the Ru atom is almost identical in both $Ru_{0.25}Ni_{0.75}(111)$ and $Ru_{0.11}Ni_{0.89}(111)$. However, the DOS near the Fermi level differs considerably. The Ru atom in $Ru_{0.25}Ni_{0.75}(111)$ and the Ni atom in $Ru_{0.11}Ni_{0.89}(111)$ have a higher density of occupied states near the Fermi level as compared to Ni atom in $Ru_{0.25}Ni_{0.75}(111)$ and the Ru atom in $Ru_{0.11}Ni_{0.89}(111)$. This explains why S adsorption energies are more favorable by 0.11 eV on the Ru-containing hollow in $Ru_{0.25}Ni_{0.75}(111)$ compared to $Ru_{0.11}Ni_{0.89}(111)$. A comparison of the DOS of a Ru atom on the surface of a homogeneous $Ru_{0.25}Ni_{0.75}(111)$ alloy and a Ru atom in an inhomogeneous alloy (see supporting information) reveals a similar favorability for S adsorption when there is an increased presence of electrons close to Fermi level. The sulfur adsorption energy on this inhomogeneous alloy is more favorable by 0.22 eV as compared to that on the homogeneous alloy.

One way to illustrate the relationship between the DOS near the Fermi level and the adsorption energy of sulfur is to plot adsorption energy versus the number of states within an arbitrary range close to the Fermi level. A strong

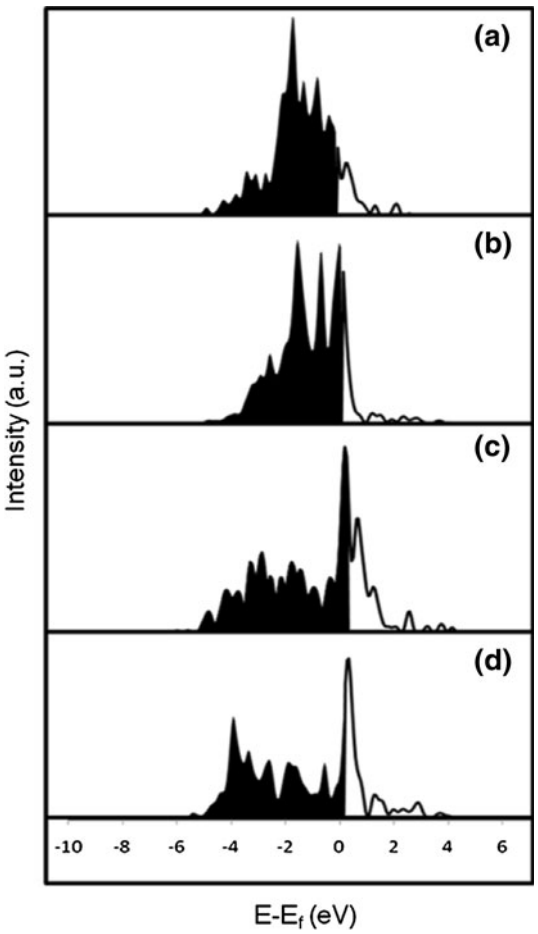

Fig. 3 DOS of the **a** Ni atom in $Ru_{0.25}Ni_{0.75}(111)$, **b** Ni atom in $Ru_{0.11}Ni_{0.89}(111)$, **c** Ru atom in $Ru_{0.25}Ni_{0.75}(111)$ and **d** Ru atom in $Ru_{0.11}Ni_{0.89}(111)$. The *shaded region* represents the occupied states and the *unshaded region* represents the unoccupied region of the d band

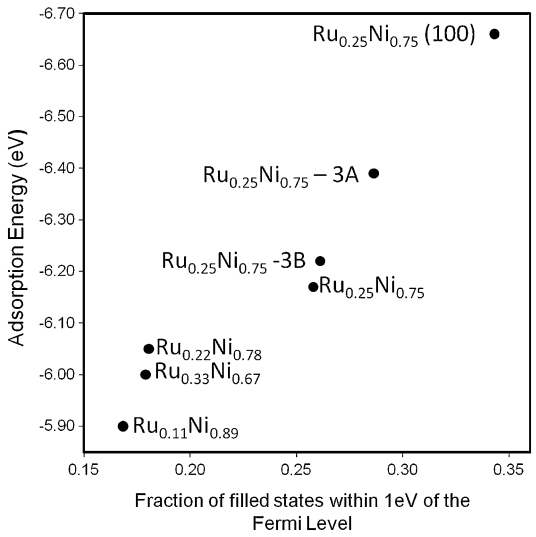

Fig. 4 S adsorption energy on the Ru hollow sites of various NiRu alloys versus the quantity of 1/3 (the fraction of states in the Ru atom) + 2/3 (the fraction of states in the Ni atom) within 1.0 eV of the Fermi level. All the alloys have a (111) face except $Ru_{0.25}Ni_{0.75}(100)$. Alloys 3A and 3B are inhomogeneous, as described in the Supporting Information

relationship between the fraction of occupied states and the S adsorption energy on the Ru hollow site of various NiRu alloys for an arbitrary 1 eV energy range below the Fermi level is found (see supporting figure S8). Though this specification is arbitrary, we find that this trend is followed regardless of the specified energy range, spanning a significant range of values. For example, a similar relationship is obtained when a 0.5 eV range below the Fermi level is used. The adsorption site for S is made up of two Ni atoms and one Ru atom, so it is expected that the electronic structure of the Ni component is also critical. The S adsorption energy was also found to be correlated with the DOS near the Fermi level of Ni. Finally, perhaps the most useful metric attempts to incorporate the presence of both Ni and Ru surface atoms in the binding site. This can be represented by taking a weighted average of the DOS near the Fermi level according to the stoichiometry of the binding site; that is, for a site consisting of two Ni atoms and one Ru atom, using the sum of 2/3 the DOS of the Ni atoms and 1/3 the DOS of the Ru atoms. This produces a strongly linear relationship, as shown in Fig. 4.

Next we consider the underlying reasons for trends in ethylene adsorption energy, which are simpler because of the simplicity of the ethylene binding site (atop a single atom). Ethylene adsorption can be described in terms of the Dewar–Chatt–Duncanson model [46, 47]. According to this model, there is a donation of electrons from the π orbital of the adsorbate to the metal d-band and a back donation from the metal to the π^* orbital of the adsorbate. An alternative view is that the activation of C_2H_4 on a metal surface is due to spin uncoupling in the adsorbate that leads to an excitation to the triplet state and thus prepares the adsorbate for bond formation [48].

We observed an increase of 0.12 Å in the C–C bond length of ethylene for both Ni(111) as well as the NiRu alloys; this expansion is in accordance with previous observations of rehybridization [49–52]. This increase in C–C bond length and the upward shift of hydrogen atoms can be attributed to the σ–π mixing that occurs when ethylene binds to the Ni or NiRu surface. The DFT results indicate that ethylene binds preferentially atop the Ru atom on the bimetallic surfaces. It is useful to consider correlations with the electronic properties of these atoms across all the bimetallic surfaces considered above. Ethylene adsorption does not correlate with the d-band center of the Ru atom on which it adsorbs (see supporting information). However, C_2H_4 adsorption is more favorable on metal atoms (in this case Ru) that have a larger density of unoccupied states near the Fermi level, as demonstrated in Fig. 5. This figure shows ethylene adsorption energy versus

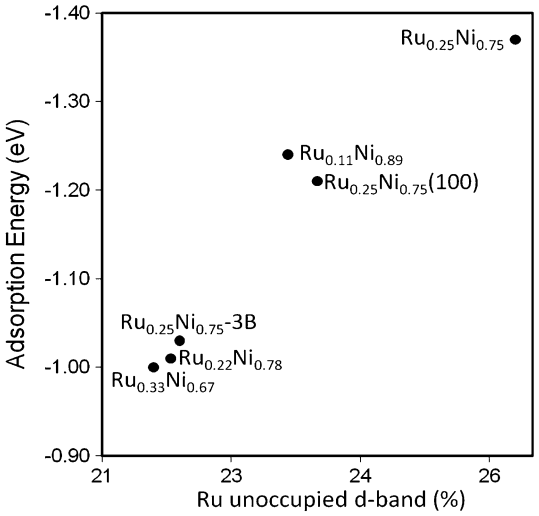

Fig. 5 C_2H_4 adsorption energy versus the percentage of unoccupied d-states near the Fermi level of the Ru atom of an alloy. All the alloys have a (111) face except $Ru_{0.25}Ni_{0.75}(100)$

the percentage of unoccupied d-states in the Ru atom of various bimetallic NiRu(111) alloys. Ethylene adsorption becomes more favorable as the percentage of unoccupied d-states in a metal atom increases. The results discussed earlier indicate that C_2H_4 adsorption becomes more exothermic as the Ru concentration in the bimetallic alloy decreases. As seen in Fig. 3, this is because of the decrease in the percentage of the unoccupied d-states with respect to the total DOS of the d-band of the Ru atom. The increase in unoccupied states reduces the anti-bonding repulsion and leads to more efficient rehybridization enabling formation of bonds to the adsorbate.

In our previous work, we found that the addition of Ru to a Ni catalyst supported on Al_2O_3 (Ni/Al_2O_3) greatly improved its activity both in the presence as well as the absence of sulfur [17]. As mentioned earlier, ethylene adsorption is favored if there are more unoccupied states above the Fermi level. The addition of Ru to a Ni catalyst increases the number of unoccupied states available for bonding above the Fermi level compared to either Ru(0001) or Ni(111) surfaces (see supporting information, Fig. S9). This, in turn, causes less repulsion during C_2H_4 adsorption on the NiRu(111) catalyst. This shift in the electronic structure that favors ethylene adsorption was observed in all the NiRu alloys investigated for this study. Moreover, sulfur adsorption is less favorable on the $Ru_{0.25}Ni_{0.75}(111)$ surface than on Ni(111). This is consistent with the observation that the Ni atom in the Ni(111) slab has 28 % of its occupied states within 1 eV of the Fermi level compared to 25 % in the Ru atom or 22 % in the Ni atom of $Ru_{0.25}Ni_{0.75}(111)$.

Overall, it appears that the enhanced reactivity of ethylene in both the presence and absence of sulfur on NiRu bimetallics may be related to the different mechanisms for ethylene and sulfur adsorption on the two surfaces. To illustrate this divergence, sulfur adsorption energies on Ni(111), $Ru_{0.25}Ni_{0.75}(111)$ and Ru(0001) are −6.77, −6.17 and −5.24 eV, respectively. Ethylene adsorption on $Ru_{0.25}Ni_{0.75}(111)$ was more favorable at −1.37 versus −0.77 and −0.89 on Ni(111) or Ru(0001), respectively. Thus, S adsorption is less favorable on the $Ru_{0.25}Ni_{0.75}(111)$ than the Ni(111) slab and ethylene adsorption is more favorable on the bimetallic than either Ni(111) or Ru(0001). This change in adsorption energy values is a direct consequence of the different electronic structure of the three surfaces as described above.

3.3 Mechanisms for Sulfur Resistant Ethylene Reforming on Bimetallic Ni-Based Catalysts

The catalytic studies presented here and elsewhere reveal that a number of Ni-based bimetallics including NiW, NiSn, NiRu, and NiRh exhibit improved sulfur resistance during hydrocarbon steam reforming reactions [9, 10, 13, 17]. However, the mechanisms for these bimetallics appear to vary significantly. The use of the bimetallic systems NiW and NiSn reduces the initial activity of the catalysts in the absence of sulfur, but also reduces the susceptibility to poisoning. The addition of Ru and Rh—metals which are themselves active catalysts—to Ni can result in higher reforming activity both in the presence and absence of sulfur, but with an improvement in the overall sulfur resistance. The fact that NiRu and NiRh catalysts involve two highly active metal components complicates analysis, but such combinations of active metals have been widely used in other applications to improve poisoning resistance [53].

One important difference between the two types of bimetallic catalysts is apparent in the TPR catalyst characterization results. The addition of Sn and W to the Ni catalysts shifts TPR features to higher temperature, whereas Ru and Rh are more easily reducible metals that lower the reduction temperature of Ni. The reducibility of the catalyst has previously been correlated with the activity toward steam reforming reactions for Ni-based systems [54]. The effects of Sn on the physical and electronic structure of Ni have been thoroughly characterized; Sn forms a surface alloy with Ni, and shifts the d-band center of neighboring Ni atoms to lower energies, reducing susceptibility to poisoning by carbonaceous species and sulfur [14, 55]. The effects of W are less clear and potentially more difficult to study. The results indicate the presence of W-containing oxide and sulfide phases under reaction conditions; these phases are much more difficult to model using computational approaches than surface or homogeneous alloys. Yet, the behavior of these NiSn and NiW

catalysts appear to be similar in their overall nature—the addition of the relatively inactive components Sn and W decrease the reducibility and reactivity of the Ni component, lowering the intrinsic rate but also significantly reducing the effect of poisoning by other species. Under conditions where poisoning is a critical consideration—where decreasing the surface coverage of a poison is expected to increase the reaction rate—the effect of these promoters can be beneficial.

In contrast, NiRu surfaces adsorb ethylene more strongly, and appear to be more active catalysts. One might expect that stronger binding of ethylene would be correlated with stronger binding of atomic sulfur, leading to poor poisoning resistance. However, ethylene and sulfur prefer different adsorption sites on the surface, and the strength of their binding is dictated by different electronic features of the surface. Because of this, surfaces can be designed to favor binding of a desired species, such as ethylene, in preference to an undesired poison, such as sulfur. Although not included in this study, we hypothesize that Rh improves the sulfur-resistant activity of Ni through a similar mechanism.

4 Summary

Experimental studies revealed that addition of W to Ni/Al_2O_3 catalysts decreases the activity of the catalyst for steam reforming of ethylene under sulfur-free conditions, but improves activity in the presence of H_2S. This behavior contrasts to previous studies of NiRu bimetallic catalysts, which showed improved ethylene stream reforming activity both in the presence and absence of sulfur. Using DFT calculations, we have demonstrated that S and C_2H_4 adsorption on NiRu bimetallic alloys is affected by several factors: Ru concentration in the NiRu alloy, the adsorption site, the face of the alloy and local surface conditions. Sulfur preferentially adsorbs on the Ru hollow site on all the NiRu(111) alloys we examined except $Ru_{0.11}Ni_{0.89}$(111). Ethylene, on the other hand, preferentially adsorbs atop the Ru atom in all the NiRu(111) alloys studied. The differences in trends observed for S and C_2H_4 adsorption on the different NiRu(111) bimetallic alloys can be attributed to the difference in the adsorption mechanisms of the adsorbates in consideration. Sulfur adsorption is dependent on the occupied d-DOS near the Fermi level while C_2H_4 adsorption is dependent on the percent of unoccupied d-DOS of the atom with respect to the total d-DOS of the metal atom. In contrast, modifiers such as W and Sn appear to function by shifting the d-band center of the Ni atoms to lower energies.

Acknowledgments Research funding from the National Renewable Energy Laboratory through subcontract KXEA-3-33606-26 and from the U.S. Department of Energy's Biomass Program Contract DE-AC36-99-GO-10337 are gratefully acknowledged. This research utilized the NCSA-Teragrid system and the high-performance computing cluster carbon at Argonne National Laboratory.

References

1. Galea NM, Lo JMH, Ziegler T (2009) J Catal 263:380
2. Sinfelt JH (1983) Bimetallic catalysis: discoveries, concepts and applications. Wiley, New York
3. Rodriguez JA (2006) Prog Surf Sci 81:141
4. Bligaard T, Norskov JK (2007) Electrochim Acta 52:5512
5. Greeley J, Norskov JK, Kibler LA, El-Aziz AM, Kolb DM (2006) ChemPhysChem 7:1032
6. Kitchin JR, Norskov JK, Barteau MA, Chen JG (2004) Phys Rev Lett 93:156801
7. Liu P, Norskov JK (2001) Phys Chem Chem Phys 3:3814
8. Mavrikakis M, Hammer B, Norskov JK (1998) Phys Rev Lett 81:2819
9. Wang LS, Murata K, Inaba M (2009) Appl Catal A 358:264
10. Strohm JJ, Zheng J, Song CS (2006) J Catal 238:309
11. Wang LS, Murata K, Inaba M (2004) Appl Catal B 48:243
12. Wang LS, Murata K, Matsumura Y, Inaba M (2006) Energy Fuels 20:1377
13. Molenbroek AM, Norskov JK, Clausen BS (2001) J Phys Chem B 105:5450
14. Nikolla E, Schwank J, Linic S (2007) J Catal 250:85
15. Ishihara A, Qian EW, Finahari IN, Sutrisna IP, Kabe T (2005) Fuel 84:1462
16. Jeong JH, Lee JW, Seo DJ, Seo Y, Yoon WL, Lee DK, Kim DH (2006) Appl Catal A 302:151
17. Rangan M, Yung MM, Medlin JW (2011) J Catal 282:249
18. Kresse G, Hafner J (1993) Phys Rev B 47:558
19. Kresse G, Furthmuller J (1996) Comput Mater Sci 6:15
20. Kresse G, Joubert D (1999) Phys Rev B 59:1758
21. Perdew JP, Yue W (1986) Phys Rev B 33:8800
22. Monkhorst HJ, Pack JD (1976) Phys Rev B 13:5188
23. He X, Kong LT, Li JH, Li XY, Liu BX (2006) Acta Mater 54:3375
24. Hyman MP, Loveless BT, Medlin JW (2007) Surf Sci 601:5382
25. Bartholomew CH, Farrauto RJ (1976) J Catal 45:41
26. Bartholomew CH, Pannell RB, Butler JL (1980) J Catal 65:335
27. Yung MM, Kuhn JN (2010) Langmuir 26:16589
28. Ravel B, Newville M (2005) Phys Scr T115:1007
29. Newville M (2001) J Synchrotron Radiat 8:322
30. Newville M (2001) J Synchrotron Radiat 8:96
31. Ashrafi M, Pfeifer C, Proell T, Hofbauer H (2008) Energy Fuels 22:4190
32. Oudar J (1980) Rev Sci Eng 22:1980
33. Barbier J, Lamy-Pitara E, Marecot P, Boitiaux JP, Cosyns J, Verna F (1990) Adv Catal 37:279
34. Rodriguez JA, Chaturvedi S, Kuhn M, Hrbek J (1998) J Phys Chem B 102:5511
35. Rodriguez JA, Hrbek J (1999) Acc Chem Res 32:719
36. Choi YM, Compson C, Lin MC, Liu ML (2007) J Alloy Compd 427:25
37. Chen YS, Xie C, Li Y, Song CS, Bolin TB (2010) Phys Chem Chem Phys 12:5707
38. Kuhn JN, Lakshminarayanan N, Ozkan US (2008) J Mol Catal A 282:9
39. Largentiere PC, Figoli NS (1997) J Chem Technol Biotechnol 69:261
40. Porto LM, Butt JB (2002) Ind Eng Chem Res 41:5420

41. Rodriguez JC, Romeo E, Fierro JLG, Santamaria J, Monzon A (1997) Catal Today 37:255
42. Sato K, FujiMoto K (2007) Catal Commun 8:1697
43. Tomishige K, Miyazawa T, Kimura T, Kunimori K, Koizumi N, Yamada M (2005) Appl Catal B 60:299
44. Hammer B, Norskov JK (1995) Nature 376:238
45. Hammer B, Norskov JK (1995) Surf Sci 343:211
46. Dewar MJS (1951) Bulletin de la societe chimnique de france 18:c79
47. Chatt J, Duncanson LA (1953) J Chem Soc 2939
48. Triguero L, Pettersson LGM, Minaev B, Agren H (1998) J Chem Phys 108:1193
49. Demuth JE, Ibach H (1978) Surf Sci 78:L238
50. Hammer L, Muller K (1990) Prog Surf Sci 35:103
51. Yilmazer ND, Fellah MF, Onal I (2010) Appl Surf Sci 256:5088
52. Brown WA, Kose R, King DA (1999) J Mol Catal A 141:21
53. Lee SA, Park KW, Kwon BK, Sung YE (2003) J Ind Eng Chem 9:63
54. Magrini-Bair KA, Czernik S, French R, Parent YO, Chornet E, Dayton DC, Feik C, Bain R (2006) Appl Catal 318:199
55. Nikolla E, Schwank J, Linic S (2009) J Am Chem Soc 131:2747